Journal of Pain Research

Dovepress
Taylor & Francis Group

Open Access Full Text Article

ORIGINAL RESEARCH

Acupotomy Activates PI3K/Akt Signaling Pathway Mediated by FGF7,10/KDR Axis to Regulate Apoptosis

Jia-Ming Qian[1], Xiao-Le Wang[1], Ting Fang[1], Lang Liu[1], Fu-Shui Liu[1,2], Xiao-Lan Zhao[2], Khaliunaa Tumurbaatar[2,3]

[1]Affiliated Hospital of Jiangxi University of Chinese Medicine, Nanchang, Jiangxi, 330006, People's Republic of China; [2]Graduate School of Jiangxi University of Chinese Medicine, Nanchang, Jiangxi, 330004, People's Republic of China; [3]Institute of Traditional Medicine and Technology, Ulan Bator, 17032, Mongolia

Correspondence: Fu-Shui Liu, Email 20050827@jxutcm.edu.cn

Objective: Acupotomy in the treatment of cervical spondylosis (CS) is effective and widely used in clinic, but the mechanism is still unclear. In this study, we started from treating CS with acupotomy "regulating muscles to treat bone disorders" and cervical myocyte apoptosis, the mechanism of acupotomy activates PI3K/Akt signaling pathway mediated by FGF7,10/KDR signaling axis to regulate apoptosis was explored, providing theoretical basis for clarifying the target and molecular mechanism of acupotomy for CS.

Methods: Seventy-four SPF SD rats were divided into 9 groups, including acupotomy group, sham operation group, model group, normal group, control AAV group, control AAV+model group, AAV+model group, and AAV+model+acupotomy group. The CS model was verified by cervical spine X-ray and transmission electron microscopy. Multiple immunofluorescence and COIP techniques were used to verify the interaction between FGF7, FGF10 and KDR proteins in splenius capitis. The tension and pain threshold of rats were measured to evaluate motor and sensory disorders. HE staining was used to observe the pathological changes of splenius capitis. Finally, the expressions of FGF7, FGF10, KDR, PI3K, Akt, bcl2 and Caspase9 were detected by qPCR and Western blot.

Results: X-ray and transmission electron microscopy showed that the CS model was successfully constructed. Multiple immunofluorescence and COIP techniques identified the interaction between FGF7, FGF10 and KDR proteins. Acupotomy can effectively improve the tension and pain threshold of CS rats and also improve cervical vertebrae degeneration. After modeling, the expressions of FGF7, FGF10, KDR and Caspase9 were increased, while the expressions of PI3K, Akt and bcl2 were decreased, which could be reversed by acupotomy. The effect is alleviated after knockdown of KDR, and the downstream signal transmission is blocked.

Conclusion: Acupotomy activates PI3K/Akt signaling pathway mediated by FGF7,10/KDR signaling axis, regulates cervical myocyte apoptosis, and repairs strained muscles, which may be the key molecular mechanism of treating CS with acupotomy "regulating muscles to treat bone disorders".

Keywords: acupotomy, cervical spondylosis, regulating muscles to treat bone disorders, FGF, KDR, apoptosis, adeno-associated virus

Introduction

Cervical spondylosis (CS) refers to cervical intervertebral disc degeneration and its secondary pathological changes of adjacent structures involving the surrounding nerves and blood vessels. CS is characterized by high incidence and long disease course.[1] With the change of modern life and work style, CS presents a general and younger trend,[2] which has a significant impact on society and economy.[3,4] The pathogenesis of CS is complex, but there are no more than "bone theory", "soft tissue injury theory" and "biomechanical balance theory".[5] Many scholars believe that the cervical muscles play an important role in maintaining the biomechanical balance and the development of CS. From the traditional bone theory change to muscles and bone balance, the muscular system has attracted more and more attention and become the focus of CS mechanism research.

https://doi.org/10.2147/JPR.S557937
Received: 2 August 2025
Accepted: 16 December 2025
Published: 8 January 2026

Graphical Abstract

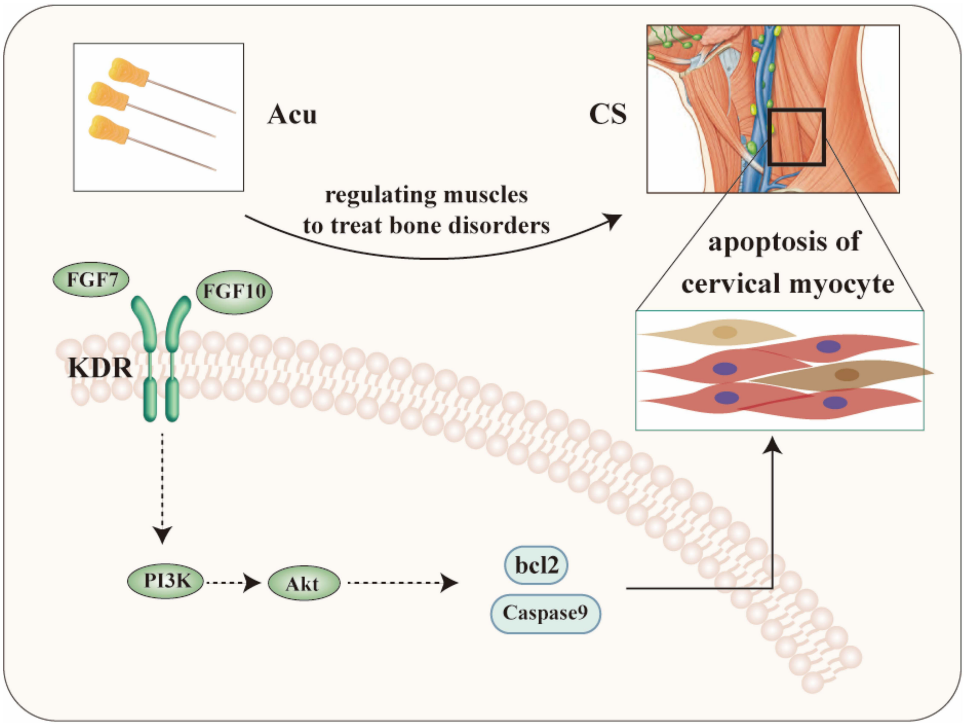

The treatment of CS includes acupotomy, acupuncture, massage, medicine and surgery. Studies have shown that 90 to 95% of patients with CS can be improved or cured with non-surgical treatment.[6,7] Acupotomy has attracted wide attention in recent years with the advantages of significant curative effect, simplicity and economy.[8] Acupotomology, founded in the late 1970s, is an organic combination of traditional Chinese medicine "acupuncture" and western medicine "scalpel" and is a retro and innovative science of acupuncture.[9] Apart from CS, acupotomy is also widely used in the treatment of musculoskeletal pain, and further studies are needed to elucidate the precise mechanisms.[10] Acupotomology believes that acupotomy treatment of CS is mainly through the role of regulating muscles, releasing adhesion, repairing injury and restoring dynamic balance. Regulating muscles can correct the bad sequence of cervical vertebra and restore static balance. Acupotomy regulates the balance of muscles and bones, restores internal and external stability, and makes the human body in a state of "bone strengthening and tendon softening"[11] In the treatment process, muscle repair is very important. Previous studies by our research group have confirmed that acupotomy may regulate cervical myocyte apoptosis by activating PI3K/Akt signaling pathway and play a role in repairing strained muscles damaged by CS.[12] Fibroblast growth factor (FGF)7,10/kinase insert domain protein receptor (KDR) signaling axis is the upstream of PI3K/Akt signaling pathway, but its key molecular mechanism is still unclear.

In order to explore the specific molecular mechanism of acupotomy treatment of CS, we used the method of unbalanced dynamic and static forces to establish CS rat model, and constructed KDR gene knockdown rats by injecting adeno-associated virus. We hope to confirm the efficacy of acupotomy for CS through animal experiments and explore the important regulatory role of FGF7,10/KDR in the repairment of strained muscles by acupotomy. This result provides an experimental basis for understanding the pathogenesis of CS and improving treatment strategies.

Materials and Methods

Animals

Seventy-four SPF SD rats, half male and half female, weighing (100±10) g, were purchased from Jiangxi University of Chinese Medicine. The SD rats were randomly assigned to 9 groups, including acupotomy group (Acu), sham operation group (Sham), model group (Model), normal group (Normal), control AAV group (ConAAV), control AAV+model group (ConAAV+M), AAV group (AAV), AAV+model group (AAV+M), and AAV+model+acupotomy group (AAV+M+Acu). There were 6 rats in each of acupotomy group, sham operation group, model group, control AAV group, and control AAV+model group, 10 rats in each of normal group and AAV group, 12 rats in each of AAV+model group and AAV +model+acupotomy group, with half male and half female. They should be allowed to eat and drink freely, ensuring that each group has the same food and water. After one week of adaptive feeding, experimental research was carried out strictly in accordance with the requirements of animal ethics. This experiment was approved by the Ethics Committee of Jiangxi University of Chinese Medicine (JZLLSC20240524). All animal experiments were conducted according to the Guidelines of the NIH for the welfare of laboratory animals.

Intervention Method

Normal group were normal fed without any intervention. Model group were adaptive fed for one week, and the dynamic and static imbalance[13] was used for modeling. Rats were anesthetized with 2% pentobarbiturate sodium at a dose of 30 mg/kg. After disinfection, a drape was spread. The skin and subcutaneous tissue were incised from the atlanto-occipital joint to the T_2 spinous process. The cervical fascia, latissimus cervicalis muscle, trapezius muscle, and rhomboid muscle were separated. Cervical spinae muscle, longest muscle, cervicoiliac rib muscle and semipinous muscle were cut. Then, separate the muscles attached to the spinous processes, laminae and facet joints on both sides of the spine and successively cut the supraspinous and interspinous ligaments of C_2-C_7. After hemostasis, suture the subcutaneous fascia and skin, as shown in Figure 1A. Penicillin (50,000 U/d) was intramuscularly injected for 3 days after the operation to prevent infection.

For sham operation group, only the skin and subcutaneous fascia were incised when dealing with the neck muscles and ligaments, without cutting the muscles and ligaments. Acupotomy treatment was performed on the rats 3 months after modeling. Firstly, the rats were fixed, and the hair on their necks were removed. After the rats calm down, perform palpation on their necks. First, determine the approximate level of the cervical vertebrae. Below the occipital bone is C_1, and by palpating downwards, the most prominent part is C_7. At the starting point of trapezius muscle, the attachment point of sternocleidomastoid muscle's mastoid process, cervical facet joints and local hard nodules or cord-like structures, depending on the stiffness and location of the hard nodules, we determined one spinous point of C_2-C_7 and two points about 0.5 cm lateral to both sides of this spinous point. Three points were the insertion points of acupotomy. The operator (the same person who has received training) should wear sterile gloves. Incision line should be parallel to the posterior midline, and the knife body should be perpendicular to the coronal plane. Press the tip of the left thumb on the needle insertion point, hold the needle knife with the right thumb and index finger, quickly and vertically insert it into the subcutaneous tissue, slowly advance the needle body to reach the bone surface, make three longitudinal cuts and two transverse strips in a small area at the lesion site, and control the cutting range within 1 mm. After completion, remove the needle and apply pressure to stop bleeding for 3 minutes. Acupotomy treatment was conducted once a week for a total of three times.

We designed three shRNA sequences targeting KDR gene knockdown and one blank control sequence. The AAV serotype is AAV2/9, and promoter driving the shRNA is U6 promoter. After packaging with AAV, they were injected into the neck of rats. Samples were collected to detect the mRNA and protein expression of KDR in the neck muscles. The shRNA sequence with the highest knockdown efficiency was selected for the formal experiment. The knockdown efficiency reached over 60%. The rats of control AAV group and AAV group were adaptive fed for 1 week, and local injection of 2*10^11 v.g. AAV or control AAV was performed. AAV or control AAV was injected in rats of control AAV +model group and AAV+model group. Dynamic and static imbalance model was established after 3 weeks. The process is shown in Figure 1B. The rats of AAV+model+acupotomy group received acupotomy treatment after AAV injection and modeling. All rats were observed simultaneously, samples were collected and indicators were detected.

Figure 1 Method of intervention in rats. (**A**) CS modeling process in rats is prepare skin, disinfect, cut the skin, fascia layer, relevant muscles and ligament, and suture the incision at last. (**B**) CS modeling process in rats after AAV injection is prepare skin, and skin was cut. The suture thread was not completely shed and absorbed. Deep fascia was cut and muscles were exposed. Muscle adhesion was visible. Muscles and ligaments of the rat were cut, and vertebral body was exposed. At last, fascia and skin were sutured. (**C**) Procedure of intervention in animal experiments.

https://doi.org/10.2147/JPR.S557937

Tension Detection

Tension of both upper limbs and limbs of rats in each group were detected at three time points, including before modeling, after modeling, and after treatment. Calibrate and zero the grip force tester, and select the Peak mode. Grasp the tail of the rats, and place them on the sensor of the tester. Keeping its upper limbs grasp the sensor while its lower limbs are suspended. Slowly pull the tail of the rat along the longitudinal axis of the sensor until its upper limbs leave the sensor, and record the maximum grip force displayed on the screen of the grip force tester. After each rat was measured three times repeatedly, the average value was taken as the tensile force of both upper limbs. When measuring the tensile force of four limbs, make the rat's limbs grasp the sensor, and slowly pull the rat's tail along the longitudinal axis of the sensor until all its limbs leave the sensor. Record the maximum grip force. After measuring each rat three times, take the average value as the tensile force of limbs. The researchers were blind of the grouping of the rats.

Pain Threshold Detection

Pain threshold was detected at three time points, including before modeling, after modeling, and after treatment. The electronic Von Frey pain measurement instrument was used for detection. The rats were placed on the metal grid plate. After they adapted for 15 minutes, the probe of the pain measurement instrument was moved to the center of the rat's sole. The pressure was continuously and linearly increased until the threshold displayed by the instrument was recorded when the rats lift their feet, avoid, and lick their feet after sensing the stimulus. Adaptability tests were conducted on all rats 3 days before modeling. When the formal test began, each rat was measured three times, and the average value was taken. The interval between each measurement was 15 minutes. The researchers were blind of the grouping of the rats.

Cervical Spine X-Ray

Cervical spine X-ray of rats in acupotomy group and AAV+model+acupotomy group were taken after anesthesia at three time points, including before modeling, after modeling, and after treatment. Considering the need to directly observe the changes of the same rat before modeling, after modeling, and after treatment, we chose rats in acupotomy group and AAV+model+acupotomy, which reduce animal harm while meeting the experimental requirements. We observed the intervertebral space, the osteophytes of the anterior and posterior margins of the vertebral body, and the facet joints. Under the same conditions, the X-rays were read collectively to observe the height of the intervertebral space, the size of the intervertebral foramen, the physiological curvature of the cervical vertebrae, the osteophytes of the anterior and posterior margins, and facet joints of the rats. The scores were conducted and statistically analyzed refering to the cervical spine X-ray scoring method.[14]

Collection of Specimens

All the animals were weighed on an empty stomach in the 21st week. The rats were intraperitoneally injected with 2% pentobarbital sodium solution for anesthesia. The skin and fascia were incited, and the bilateral captaris muscles were located. A 1 mm^3 size muscle tissue was cut with a scalpel. The tissue was placed in the fixative of the electron microscope and fixed at room temperature for 2 hours. The remaining part should be soaked in the tissue fixative for more than 24 hours. The other piece was divided into two parts. One half was placed in a cryotube with RNA preservation solution, and the other half was placed in a common cryotube. After rapid freezing with liquid nitrogen, it was transferred to −80°C refrigerator for subsequent detection. The rats were sacrificed by excessive anesthesia. The intervention process of animal experiments is shown in Figure 1C.

Transmission Electron Microscopy

The tissue samples in the electron microscope fixative were taken out, rinsed with 0.1M phosphate buffer PB, fixed at room temperature in the dark with 1% osmium acid. Dehydrate the tissue samples in gradient alcohol and 100% acetone. After the penetration embedding was carried out, the embedding plate was placed in a 60°C oven for polymerization for 48 hours. The resin blocks were cut into 1.5 μm thick pieces using semi-thin slicing machine, stained with toluidine blue, and positioned under light microscope. The resin blocks were cut into 60 nm thick slices using ultra-thin slicer and

scooped with copper mesh. The copper mesh was stained in 2% saturated alcohol solution of uranium acetate and 2.6% lead citrate solution. Finally, under the transmission electron microscope, images of sarcoids, mitochondria, and apoptotic body were collected to analyze the ultrastructural changes of splenius capitis.

Multiple Immunofluorescence

Multiplex immunofluorescence detection was performed on splenius capitis of rats in normal group and model group. The muscle tissues were removed from the tissue fixative, trimmed neatly, and placed in the embedding frame. After the steps of dehydration, transparency and wax immersion, paraffin embedding was carried out. The cross-section of the muscle tissue was parallel to the embedding surface. After slicing, scooping, roasting and dewaxing to water, antigen repair was carried out. 3% hydrogen peroxide solution was added dropwise to block endogenous peroxidase, and 3%BSA was added dropwise for serum blocking. The KDR primary antibody was incubated overnight, and the corresponding species HRP-labeled secondary antibody was dropped in. After incubation at room temperature, the corresponding TSA fluorescent dye (IF440, cyan) was dropped in, and the incubation was carried out at room temperature in the dark. The slices were putted into the citric acid repair solution, heated in the microwave oven, and blocked by serum again. The steps of adding the second primary antibody (FGF7), adding the secondary antibody, adding TSA fluorescent dye (IF555, red), and microwave process were same with the above. The steps of adding the third primary antibody (FGF10), adding the secondary antibody, and adding TSA fluorescent dye (IF647, yellow) were same with the above. After being re-stained with DAPI and quenched by autofluorescence, the slices were sealed. Finally, fluorescence filter imaging of the corresponding wavelengths was carried out in sequence, and co-localization analysis was performed using Image J software.

COIP

COIP detection was performed on splenius capitis of rats in normal group and model group. The samples were taken out and chopped. Then protease inhibitors and IP lysis buffer were added. Homogenization was carried out using a high-throughput cryogenic grinder. After centrifugation, the supernatant was collected into Input group. IgG and protein A/G beads were mixed thoroughly and added into IgG group samples. In the COIP group, only protein A/G beads were added. After incubation, the supernatant was obtained by centrifugation. KDR primary antibody was added and incubated overnight. The beads were added and incubated at low temperature. Immunoprecipitation complex was collected by centrifuge. Then it was washed with IP lysis buffer and centrifuged to remove the supernatant, repeated 4 times. Finally, we added reduced sample loading buffer, centrifuged and took the supernatant for WB detection. The supernatant was added to the sample wells of IgG group and COIP group, respectively, and the protein detection of target proteins (FGF7, FGF10, and KDR) was carried out simultaneously with Input group. Finally, image analysis was conducted on the obtained WB strips by Image J software.

HE Staining

The paraffin sections obtained in multiplex immunofluorescence detection were stained with hematoxylin, rinsed, placed in the differentiation solution, washed with distilled water, and then stained in eosin staining solution. After dehydration and transparency, sealing was carried out. The pathological changes of the cross-sectional area of splenius capitis were observed under the microscope. The researchers were blind of the grouping of the rats.

qPCR

100 mg of the rat splenius capitis tissue was grinded thoroughly in a mortar. RNA was extracted according to the steps in the reagent manual. RNA concentration was detected. Overly concentrated RNA was diluted in an appropriate proportion to make its final concentration 200 ng/μL. 10 μL of total RNA was took out and prepared into 20 μL reaction system. It was gently mixed and centrifuged, and we completed reverse transcription on a common PCR instrument. 2 μL of the reverse transcription and 1.5 μL of the primer system were prepared into a 15 μL reaction system. The primer sequence is shown in Table 1. Amplification was completed on a fluorescence quantitative PCR instrument, and the results were analyzed by the relative quantitative $2^{-\Delta\Delta Ct}$ method.[15] The researchers were blind of the grouping of the rats.

Table 1 Primer Sequence

Gene Name	Primer Sequence (5'→3')	Length of Production (bp)
FGF7	F:CAAAGGGGTGGAAAGTGAATAC R:GTGTGTCCATTTAGCTGATGCA	145
FGF10	F:CATCAGTGGAAATCGGAGTTGT R:ACATACATTTGCCTGCCGTTG	193
KDR	F:CAAGTCCGAATCCCTGTGAAGT R:GGTGAGGATGACCGTGTAGTTTC	165
PI3K	F:TGGCTTACGCTCCAGTATTTGC R:TAGAAGTGGGCTTGGGTGGTTTA	241
Akt	F:CGCTTCTTTGCCAACATCG R:CACTGGCTGAGTAGGAGAACTGG	217
Bcl2	F:TTGTGGCCTTCTTTGAGTTCG R:GCATCCCAGCCTCCGTTAT	151
Caspase9	F:GACCAATGGGACTCAAATCAAAG R:TCGATCTTCCCTGGAGTACAGAC	208
GAPDH	F:CTGGAGAAACCTGCCAAGTATG R:GGTGGAAGAATGGGAGTTGCT	138

Western Blot

20 mg of rat muscle tissue was cut into small pieces. Lysis buffer was added for grinding and homogenization. The supernatant was obtained by centrifuge which is for protein quantification. The protein concentration of the sample was determined in accordance with the instructions of the BCA protein Quantitative Detection Kit. PBS was added for protein concentration normalization. Gel was prepared in accordance with the instructions of the one-step PAGE Color Gel Ultra-rapid Preparation Kit. After electrophoresis, membrane transfer and blocking with protein-free rapid blocking solution, the primary antibody was added, and the membrane protein was placed face down on the surface of the antifluid and incubated overnight. After washing with TBST membrane washing solution, secondary antibody incubation was carried out. After the images were displayed by the ECL luminescence method, photos were taken. The grayscale values were read using the Image J software. The researchers were blind of the grouping of the rats.

Statistical Analysis

Data statistical analysis was conducted using SPSS 25.0. Measurement data conforming to the normal distribution were expressed as mean ± standard deviation ($\bar{x} \pm s$). When comparing two groups and meeting the conditions of normal distribution and homogeneity of variance, the two-independent sample *t*-test was adopted. One-way ANOVA test followed by LSD was used for pairwise comparisons among multiple groups satisfied the normal distribution and homogeneity of variance. P value < 0.05 was considered statistically significant.

Results

The General Situation of Rats in Each Group

During the experiments of all 74 rats, one died of excessive anesthesia during the injection of AAV, one was euthanized after bilateral lower limb paralysis caused by spinal cord injury during the modeling process, and one died of accidental asphyxia during the feeding process. The data of 71 rats obtained were included in the analysis.

Verification of CS Model in Rats

Anteroposterior and lateral X-rays of the cervical vertebrae of the same batch of rats were taken before and after modeling, as shown in Figure 2A. In the statistical analysis of cervical X-ray scores, the score after modeling was significantly higher than that before modeling ($P < 0.05$), as shown in Figure 2B. Transmission electron microscopy observation showed that compared with the ultrastructure of normal rat splenius capitis, the muscle segments of the

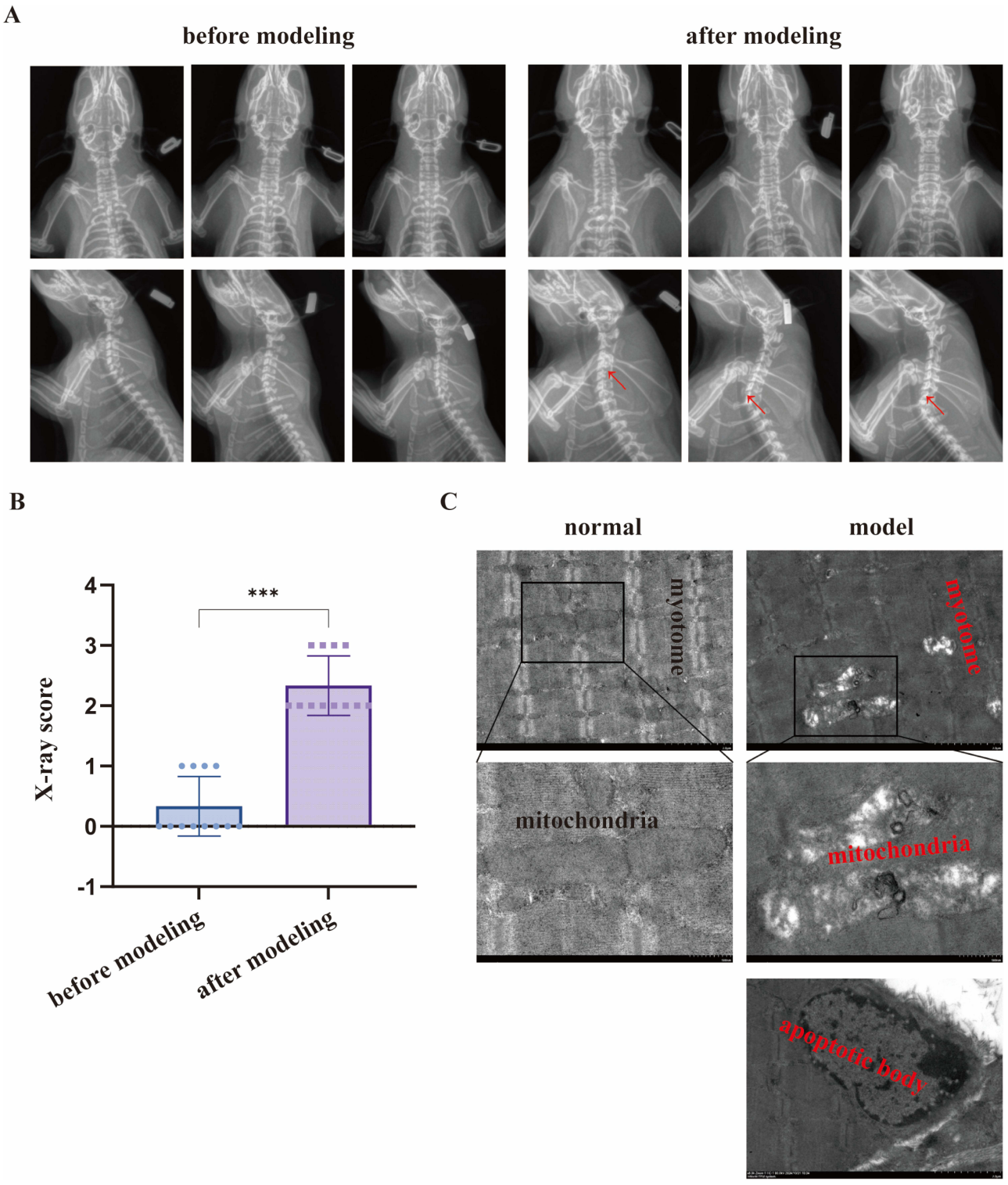

Figure 2 Verification of CS model in rats. (**A**) Anteroposterior and lateral X-rays of the cervical vertebrae in rats. (**B**) X-ray score. (**C**) Ultrastructure of splenius capitis under transmission electron microscopy.
Note: ***Indicates $P < 0.001$, red arrow indicates intervertebral disc degeneration in the X-rays.

model group were distorted and disordered after modeling. Mitochondrial structure dissolved, and there was a tendency of apoptosis. A small number of apoptotic body could be observed, as shown in Figure 2C. The results of X-rays and transmission electron microscopy verified the establishment of CS model.

https://doi.org/10.2147/JPR.S557937

FGF7 and FGF10 are Combined with KDR

Multiple immunofluorescence observation revealed that FGF7, FGF10 and KDR proteins were mainly distributed on the membranes of muscle cells, and it was more obvious in model group. Co-localization analysis indicated that in both normal group and model group, the co-localization Pearson coefficients of FGF7 and KDR were greater than 0.5 (0.65 and 0.72, respectively); The co-localization Pearson coefficients of FGF10 and KDR were also both greater than 0.5 (0.55 and 0.54 respectively). The results show that co-localization exists among FGF7, FGF10 and KDR proteins both normal and after modeling, as shown in Figure 3A. The COIP results indicated that FGF7, FGF10 and KDR proteins could be detected in input group of both normal group and model group, which proved the existence of above proteins. None of above proteins were detected in control IgG group, while COIP group tissues pulled down by magnetic beads with KDR antibody could not only detect the presence of KDR, but also the presence of FGF7 and FGF10, as shown in Figure 3B. This result directly proves that under normal condition and after modeling, there is binding and interaction between FGF7, FGF10 and KDR proteins, further promoting signal transmission.

Effective Treatment of CS by Acupotomy and Its Influence on Signaling Pathway

The data of each group, including acupotomy group, model group, sham operation group and normal group, were compared to illustrate the effective treatment of CS by acupotomy and its influence on signaling pathway.

Acupotomy Improves the Symptoms of CS

Before modeling (at the 5th week), there was no significant difference in the tension of both upper limbs among each group of rats ($P > 0.05$). After modeling (at the 18th week), tension of model group and acupotomy group was lower than that of normal group and sham operation group ($P < 0.05$). After treatment (at the 21st week), tension of acupotomy group was significantly increased compared with that before ($P < 0.05$), as shown in Figure 4A. Before modeling (at the 5th week), there was no significant difference in the tension of limbs among each group of rats ($P > 0.05$). After modeling (at the 18th week), tension of model group and acupotomy group was lower than that of normal group and sham operation group ($P < 0.05$). After treatment (at the 21st week), tension of acupotomy group was significantly increased compared with that before ($P < 0.05$), as shown in Figure 4B. Before modeling (at the 5th week), there was no significant difference in the pain threshold among each group of rats ($P > 0.05$). After modeling (at the 18th week), pain threshold in model group and acupotomy group was lower than that in normal group and sham operation group ($P < 0.05$). After treatment (at the 21st week), pain threshold in acupotomy group was significantly increased compared with that before ($P < 0.05$), as shown in Figure 4C. From the experimental results, acupotomy treatment can improve tension and pain threshold of rats with CS.

Acupotomy Improves Cervical Vertebrae Degeneration

After acupotomy treatment, X-rays in acupotomy group were taken. In the statistical analysis of X-ray scores, the score after treatment was significantly lower than that after modeling ($P < 0.05$), as shown in Figure 4D. The X-ray images of the rats after modeling and treatment were compared, as shown in Figure 4E.

Acupotomy Repairs the Strained Muscles

The morphology of muscle cells in normal group and sham operation group was normal, the arrangement was regular, and there was no infiltration of inflammatory cells. The muscle texture in model group and acupotomy group was disordered, accompanied by inflammatory cell infiltration, as shown in Figure 4F.

The Influence of Acupotomy on Signaling Pathway

The statistical analysis of relative expression level of mRNA is shown in Figure 4G. When comparing normal group with sham operation group, except for FGF10 and PI3K, there was no significant difference in mRNA expression levels ($P > 0.05$). The mRNA expression levels of FGF7, FGF10, KDR and Caspase9 in sham operation group and acupotomy group were all lower than those in model group ($P < 0.05$), while the mRNA expression levels of PI3K, Akt and bcl2 were all higher than those in model group ($P < 0.05$).

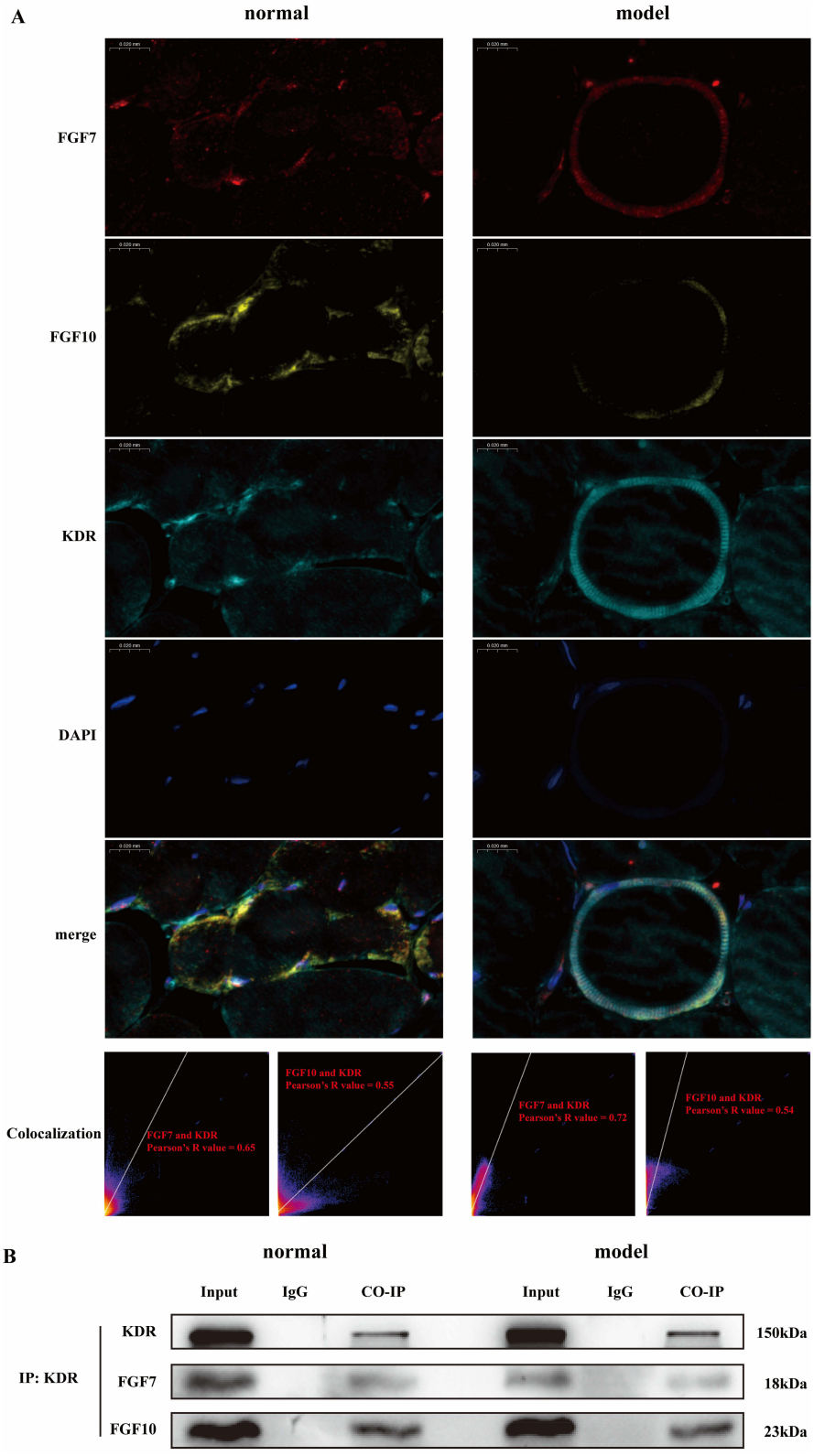

Figure 3 There are binding effects between FGF7, FGF10 and KDR. (**A**) In multiple immunofluorescence, FGF7, FGF10 and KDR proteins are co-localized. (**B**) In COIP, there are protein and protein interaction between FGF7, FGF10 and KDR.

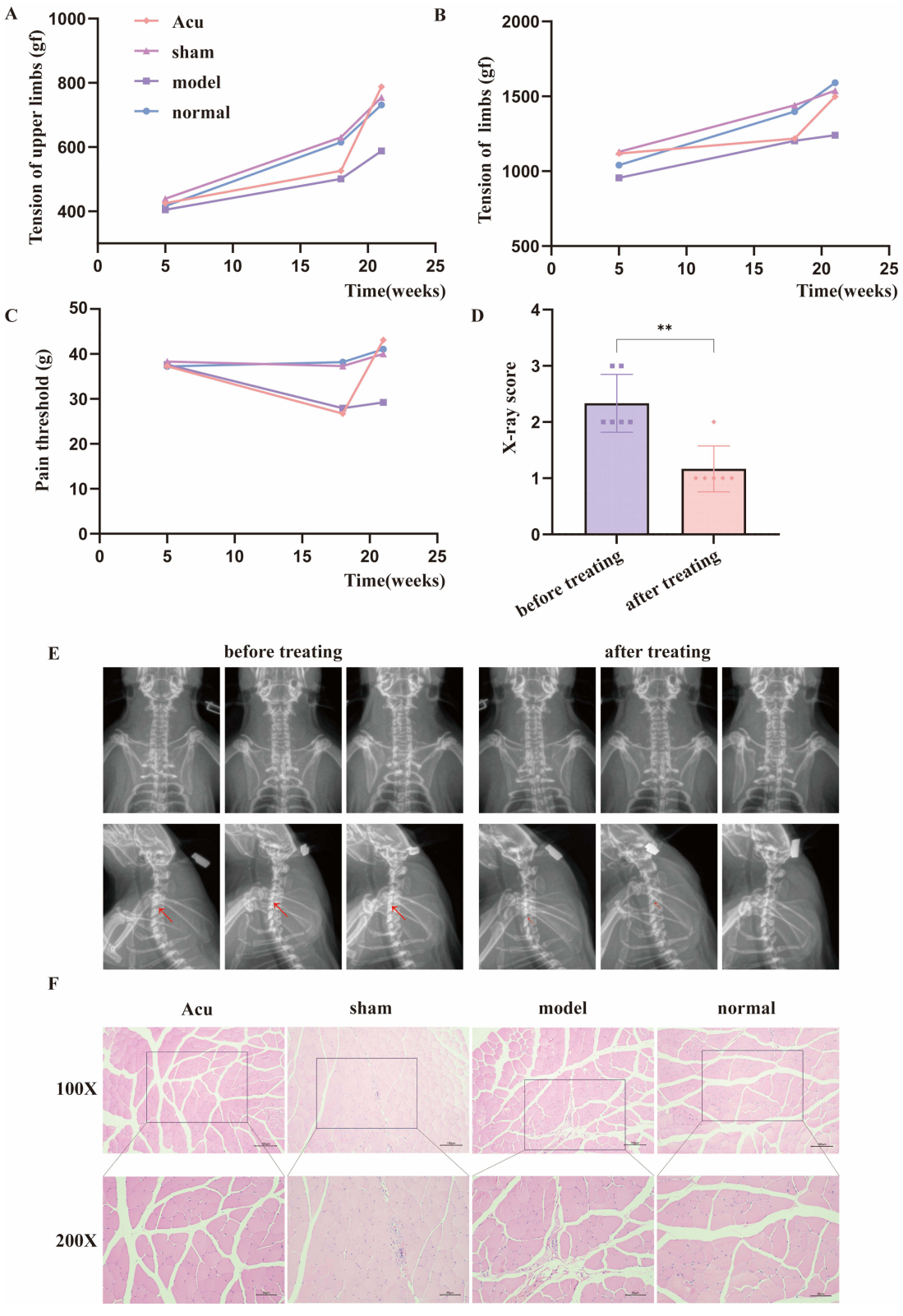

Figure 4 Continued.

https://doi.org/10.2147/JPR.S557937

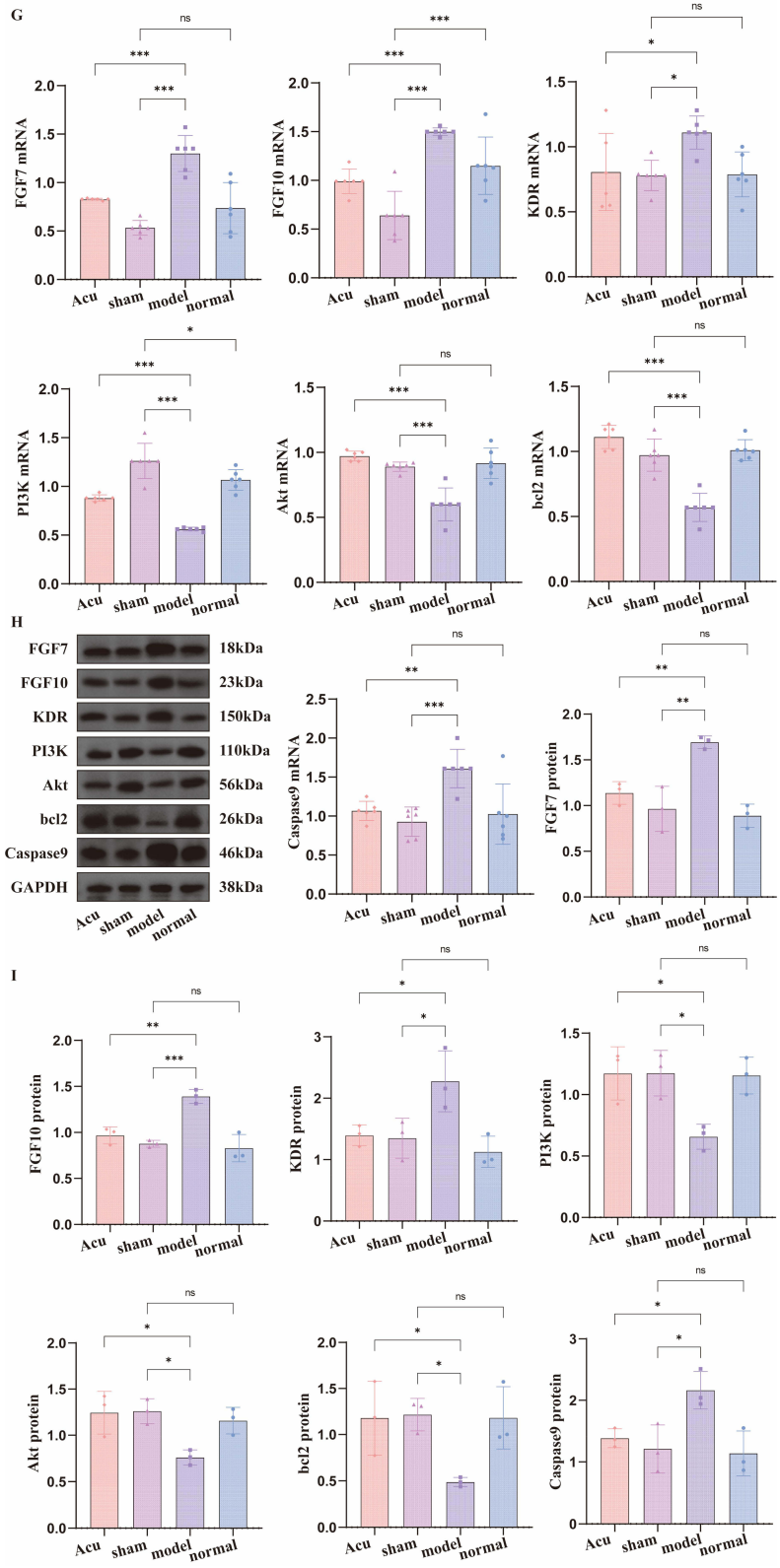

Figure 4 Effective treatment of CS by acupotomy and its influence on signaling pathway. (**A**) Changes in tension of both upper limbs. (**B**) Changes in tension of limbs. (**C**) Changes in pain threshold. (**D**) X-ray score. (**E**) Anteroposterior and lateral X-rays of the cervical vertebrae of rats in acupotomy group after modeling and treatment. (**F**) HE staining of splenius capitis. (**G**) Relative expression level of mRNA. (**H**) WB band. (**I**) The relative expression level of protein.

Notes: ns indicates no statistically significant difference, * indicates $P < 0.05$, ** indicates $P < 0.01$, *** indicates $P < 0.001$, red arrow indicates intervertebral disc degeneration in the X-rays.

The WB bands are shown in Figure 4H. The statistical analysis of the relative expression levels of proteins is shown in Figure 4I. There was no significant difference in mRNA expression levels between normal group and sham operation group ($P > 0.05$). The mRNA expression levels of FGF7, FGF10, KDR and Caspase9 in sham operation group and acupotomy group were all lower than those in model group ($P < 0.05$), while the mRNA expression levels of PI3K, Akt and bcl2 were all higher than those in model group ($P < 0.05$).

Acupotomy Mediates FGF7,10/KDR Signaling Axis, Activates PI3K/Akt Signaling Pathway, and Regulates Apoptosis

By comparing the data of rats in control AAV group, control AAV+model group, AAV group, AAV+model group, and AAV+model+acupotomy group, it is indicated that acupotomy may mediate the activation of PI3K/Akt signaling pathway by FGF7 and 10/KDR signaling axis to intervene in the apoptosis of muscle cells.

After KDR Was Knocked Down, the Effect of Acupotomy on Improving Symptoms of CS Was Alleviated

Before modeling (at the 5th week), there was no significant difference in the tension of both upper limbs among each group of rats ($P > 0.05$). After modeling (at the 18th week), tension in control AAV+model group and AAV+model group was lower than that in control AAV group and AAV group ($P < 0.05$). After treatment (at the 21st week), there was no significant improvement in AAV+model+acupotomy group ($P > 0.05$), as shown in Figure 5A. Before modeling (at the 5th week), there was no significant difference in the tension of limbs among each group of rats ($P > 0.05$). After modeling (at the 18th week), the tension in control AAV+model group and AAV+model group was lower than that in control AAV group and AAV group ($P < 0.05$). After treatment (at the 21st week), there was no significant improvement in tension in AAV+model+acupotomy group ($P > 0.05$), as shown in Figure 5B. Before modeling (at the 5th week), there was no significant difference in the pain threshold among each group of rats ($P > 0.05$). After modeling (at the 18th week), the pain threshold in control AAV+model group and AAV+model group was lower than that in control AAV group and AAV group ($P < 0.05$). After the treatment (at the 21st week), there was no significant improvement in the pain threshold in AAV+model+acupotomy group ($P > 0.05$), as shown in Figure 5C. From the experimental results, it can be seen that acupotomy treatment after knockdown of KDR has no significant improvement effect on tension and pain threshold of rats with CS.

After KDR Was Knocked Down, the Effect of Acupotomy on Improving Cervical Vertebrae Degeneration Was Alleviated

After acupotomy treatment, X-rays of rats in AAV+model+acupotomy group were taken. In the statistical analysis of X-ray scores, there was no significant difference in the scores after treatment compared with those after modeling ($P < 0.05$), as shown in Figure 5D. The X-ray images after modeling and treatment were compared, as shown in Figure 5E.

After KDR Was Knocked Down, the Effect of Acupotomy on Repairing the Strained Muscles Was Alleviated

The morphology of muscle cells in control AAV group and AAV group was normal, the arrangement was regular, and there was no inflammatory cell infiltration. The muscle texture was disordered in control AAV+model group, AAV +model group and AAV+model+acupotomy group, accompanied by inflammatory cell infiltration, as shown in Figure 5F.

After KDR Was Knocked Down, Transmission of Downstream Signaling Pathway Was Effectively Blocked

When comparing control AAV group with AAV group, control AAV+model group with AAV+model group, there was no significant difference in the mRNA expression levels of FGF7 and FGF10 ($P > 0.05$), while when comparing AAV +model group with AAV+model+acupotomy group, the latter was significantly lower than the former ($P < 0.05$). When comparing control AAV group with AAV group, control AAV+model group with AAV+model group, the mRNA expression level of KDR in the latter was lower than the former ($P < 0.05$), showing knockdown effect. However, when comparing AAV+model group with AAV+model+acupotomy group, there was no significant difference in the mRNA expression level of KDR ($P > 0.05$). Except for PI3K compared AAV+model group and AAV+model+acupotomy group, there were no significant differences in the mRNA expression levels of PI3K, Akt, bcl2 and Caspase9 between control AAV group and AAV group, control AAV+model group and AAV+model group, and AAV+model group and

 https://doi.org/10.2147/JPR.S557937

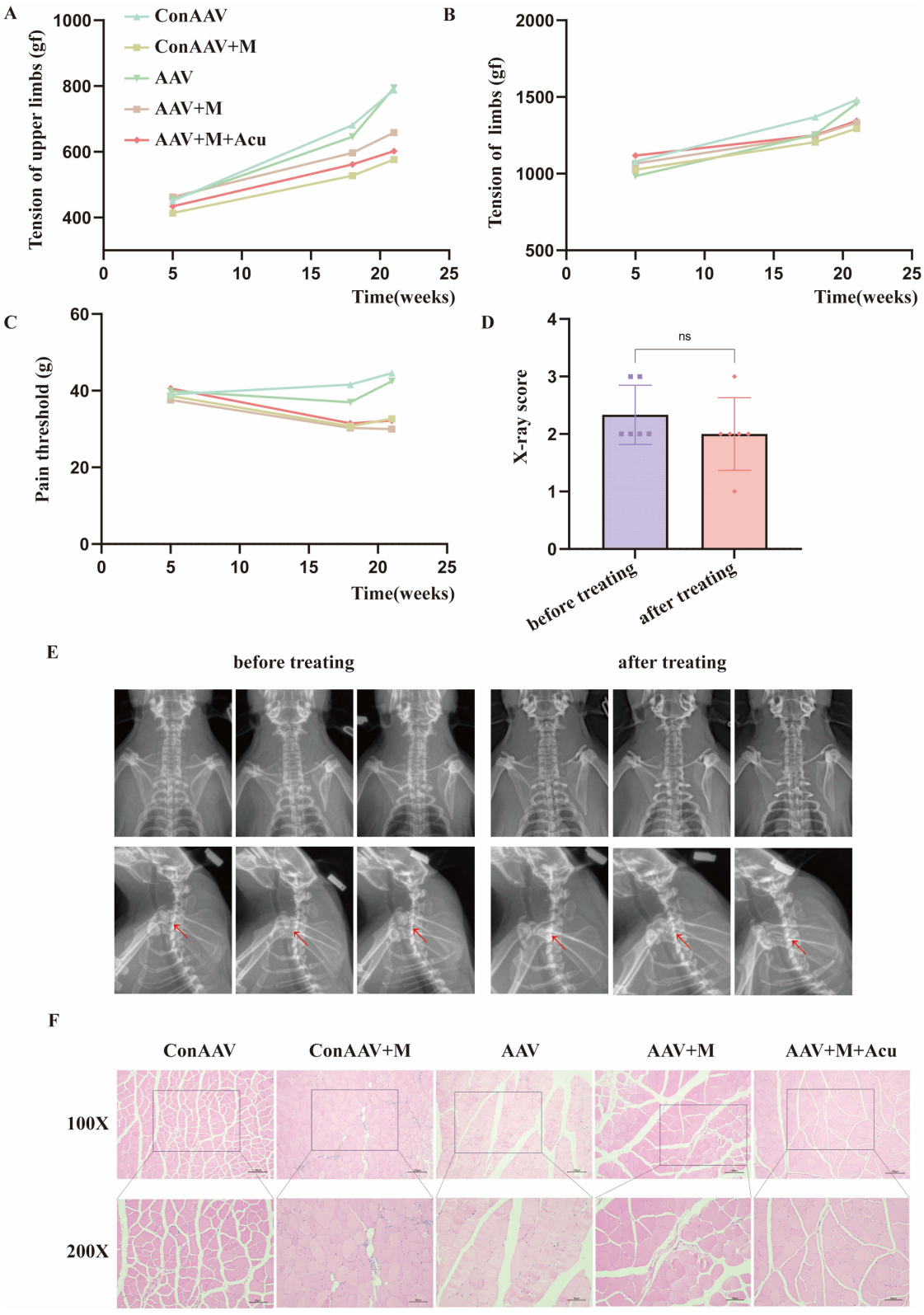

Figure 5 Continued.

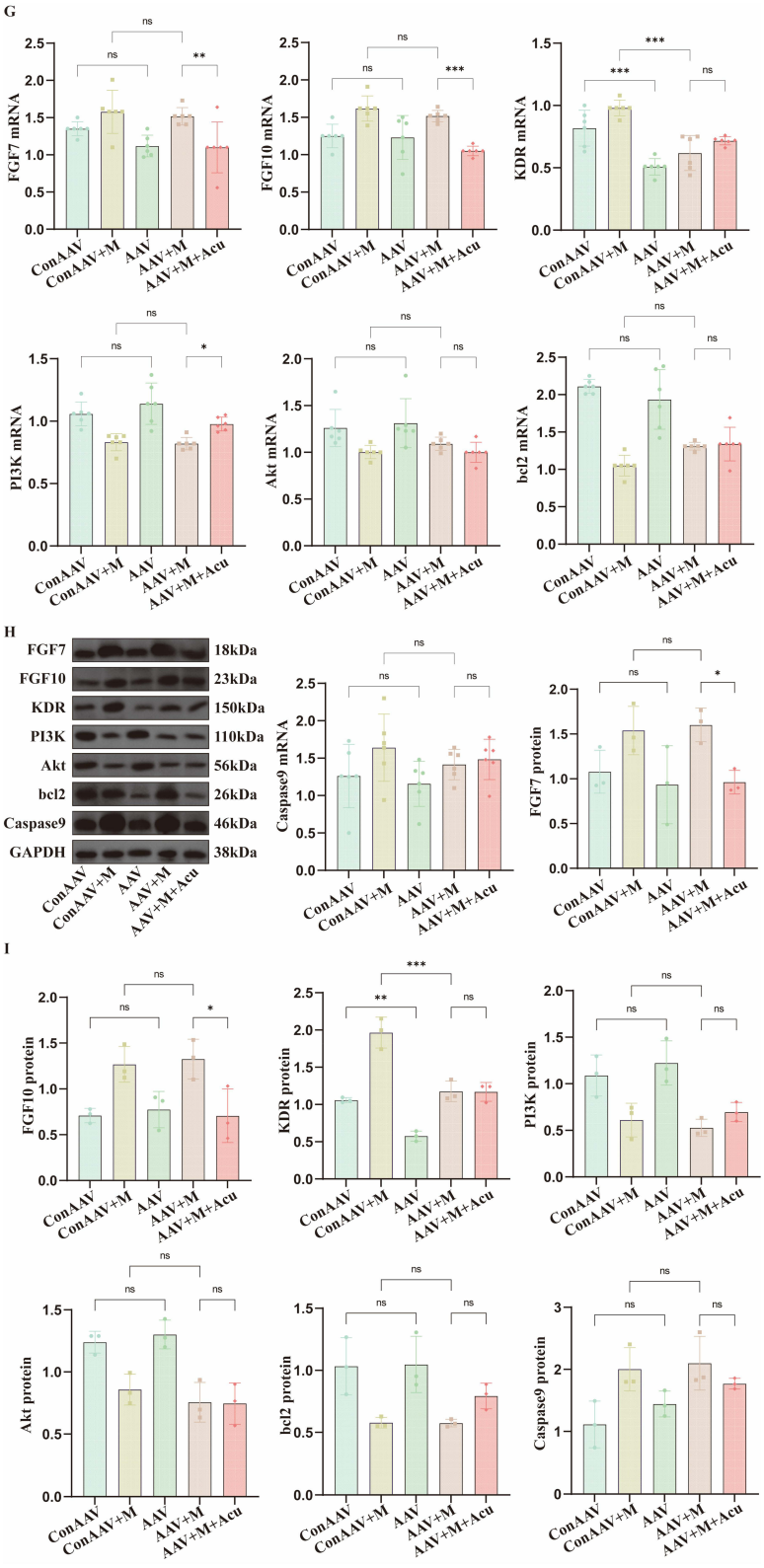

Figure 5 Acupotomy mediates FGF7,10/KDR signaling axis, activates PI3K/Akt signaling pathway, and regulates apoptosis. (**A**) Changes in tension of both upper limbs. (**B**) Changes in tension of limbs. (**C**) Changes in pain threshold. (**D**) X-ray score. (**E**) X-rays of rats in AAV+model+acupotomy group after modeling and treatment. (**F**) HE staining. (**G**) Relative expression level of mRNA. (**H**) WB band. (**I**) Relative expression level of protein.

Notes: ns indicates no statistically significant difference, * indicates $P < 0.05$, ** indicates $P < 0.01$, *** indicates $P < 0.001$, red arrow indicates intervertebral disc degeneration in the X-rays.

https://doi.org/10.2147/JPR.S557937

AAV+model+acupotomy group ($P > 0.05$), as shown in Figure 5G. It is indicated that the effect of acupotomy treatment may influence downstream signal transmission through KDR.

The WB bands are shown in Figure 5H. When comparing control AAV group with AAV group, control AAV+model group with AAV+model group, there was no significant difference in the protein expression levels of FGF7 and FGF10 ($P > 0.05$), while when comparing AAV+model group with AAV+model+acupotomy group, the latter was significantly lower than the former ($P < 0.05$). When comparing control AAV group with AAV group, control AAV+model group with AAV+model group, the protein expression level of KDR in the latter was lower than the former ($P < 0.05$), showing knockdown effect. However, when comparing AAV+model group with AAV+model+acupotomy group, there was no significant difference in the protein expression level of KDR ($P > 0.05$). There were no significant differences in the protein expression levels of PI3K, Akt, bcl2 and Caspase9 between control AAV group and AAV group, control AAV +model group and AAV+model group, and AAV+model+acupotomy group ($P > 0.05$), as shown in Figure 5I. Combined with the results of qPCR, it further indicates that the effect of acupotomy treatment may influence downstream signal transmission through KDR.

Discussion

Effect of Knocking Down KDR on Acupotomy Treatment

The targeted and precise nature of acupotomy in addressing specific trigger points and promoting tissue healing offers a promising approach for managing musculoskeletal pain. Acupotomy for CS works in the same way.

A total of 9 groups were designed in this study, including acupotomy group, sham operation group, model group, normal group, control AAV group, control AAV+model group, AAV group, AAV+model group, and AAV+model +acupotomy group. The purpose of the first four groups is to prove the success of model establishment and the effect of acupoptomy treatment on CS. The purpose of the last five groups is to prove the effect and function of knocking down KDR through inter-group comparisons. The comparison between control AAV group and AAV group proved the effect of knocking down KDR. By comparing control AAV+model group with AAV+model group, the effect of knocking down KDR combined with modeling was proved. Finally, by comparing acupotomy group with AAV+model+acupotomy group, the effect of knocking down KDR on acupotomy treatment and the changes in the downstream signaling pathways was proved. In terms of evaluation indicators, behavioral indicators such as tension of both upper limbs and limbs and pain threshold, X-rays, pathological morphology indicators such as HE staining and transmission electron microscopy, and molecular biological detection indicators such as multiple immunofluorescence, COIP, qPCR and Western blot were designed. The therapeutic effect and molecular expression of acupotomy on CS rats were explained from multiple dimensions and perspectives.

CS is often accompanied by motor and sensory disorders. In the behavioral evaluation of rats, tension of upper limbs and limbs was used to evaluate their motor disorders, and pain threshold was used to evaluate sensory disorders. After modeling, the detection indicators of rats decreased, indicating the success of modeling. The corresponding indicators improved after acupotomy treatment, suggesting that acupotomy can effectively treat CS. However, after knocking down KDR, acupotomy treatment had no obvious therapeutic effect. Cervical vertebrae degeneration and the pathological changes of splenius capitis were observed by X-ray scores and HE staining, presenting results similar to behavior indicators. Judging from the results, knocking down KDR directly affects the effect of acupotomy treatment, indicating that KDR plays a key role in the process of acupotomy treatment for CS.

FGF7,10/KDR Signaling Axis is the Key to Repair Strained Muscles with Acupotomy

As a branch of large family of growth factors, FGF is a mitogenic agent for various cell types,[16] and it affects both myogens and endothelial cells. Previous studies have shown that bFGF is an effective pro-cell division agent for endothelial cells in vitro and it stimulates angiogenesis in vivo.[17] The expression of bFGF mRNA in skeletal muscle decreases with the increase of age.[18] Interestingly, studies in vitro have demonstrated that bFGF can enhance the expression of VEGF[19] and KDR,[20] suggesting that bFGF can affect the VEGF signaling pathway and exert a synergistic effect on angiogenesis. In a study on increasing muscle strength through vertical vibration, the expression of FGF7

increased, initiating myogenesis, promoting the formation of muscle cells and myotubes, and enhancing muscle strength and bone mineral density.[21] FGF7 increases the expression of E11 in osteoblasts, promotes dendritic elongation of osteoblasts and the formation of functional space junctions, thereby playing an important role in bone development and its dynamic balance.[22] Existing studies have proved that the expression of FGF10 increases after muscle stretching.[23] FGF10 can inhibit synovial fibrosis and delay the progression of osteoarthritis.[24] In our previous study,[25] the expressions of FGF7 and FGF10 in CS rats increased after modeling, but decreased after acupotomy treatment, which was consistent with results of this study.

VEGF exerts its biological effects through Flt-1 and KDR,[26] which exhibit significantly different signal transduction and biological characteristics. Flt-1 is expressed in both proliferating and quiescent endothelial cells of adult animals, suggesting the role of this receptor in maintaining endothelial cells.[27] Meanwhile, KDR is regarded as the main mediator of VEGF on endothelial cells,[28] and it participates in the survival of endothelial cells by activating the PI3K/Akt signal transduction pathway,[29] which is considered to play an important role in inhibiting apoptosis.[30–32] The activation of VEGF/KDR signaling pathway may play an important regulatory role in maintaining capillary supply.[33]

Existing studies[34] have shown that FGF may enhance angiogenesis in fat transplantation by combining with KDR. The FGF/KDR/CSF1R signaling pathway plays a key role in the pathogenesis of multiple sclerosis. Inhibiting the expression of this pathway can effectively reduce inflammation and neurodegeneration and promote myelin regeneration.[35] Therefore, FGF7 and FGF10 may play corresponding roles by combining with KDR and further transmitting signals. In this study, multiple immunofluorescence technology was used to label the protein expressions of FGF7, FGF10 and KDR. Through co-localization analysis, it was proved that there might be co-localization among FGF7, FGF10 and KDR. The protein interaction relationships among FGF7, FGF10 and KDR were further verified by COIP. Based on the above research results and literature support, we believe that FGF7 and 10/KDR signaling axis is the key to repair strained muscles with acupotomy.

PI3K/Akt Signaling Pathway Regulates Apoptosis

PI3K/Akt signaling pathway is one of the important transduction pathways in cells and is closely related to life process such as apoptosis.[36] PI3K/Akt signaling pathway consists of PI3K and Akt. PI3K is an important component of phosphatidylinositol kinases. According to the differences in substrate specificity, structure and function, it is classified into types I, II and III. Type I exists in various cells and has been widely studied. It can be activated by tyrosine kinases (RTKs) on the cell surface.[37] The KDR in this study is a type of RTK. Akt, namely protein kinase B, is divided into three types, Akt1, Akt2, and Akt3.[38] As the main downstream target of PI3K, it can prevent cell apoptosis by inhibiting the expression of apoptotic proteins. Akt phosphorylats FOXO transcription factor to prevent it from entering nucleus and initiating the expression of pro-apoptotic genes (such as Bim, FasL).[39] Akt phosphorylates BAD to separate it from bcl-2/bcl-XL, thereby inhibiting the mitochondrial release of cytochrome C and apoptosis-inducing factor (AIF). In addition, Akt inhibits the activation of Caspase-9 and blocks the activation of downstream Caspase-3.[40]

PI3K/Akt signaling pathway can promote the proliferation and differentiation of muscle satellite cells, inhibit the apoptosis of skeletal muscle cells, and promote the regeneration and repair of skeletal muscle.[41] We have previously demonstrated the significant role of PI3K/Akt signaling pathway in the acupotomy treatment for CS. In the CS rabbit model, the protein expressions of PI3K and p-Akt were significantly downregulated, and the apoptosis of posterior cervical extensor cells increased. Acupotomy treatment restored the autophagy-apoptosis balance by activating PI3K/Akt pathway, up-regulating mRNA levels of PI3K and p-Akt.[12] Meanwhile, exogenous Adropin[42] significantly improved muscle injury by activating KDR/PI3K/Akt pathway, reducing oxidative stress, promoting microangiogenesis, inhibiting myocardial fibrosis and apoptosis. It is indicated that KDR can act as an upstream molecule of PI3K/Akt pathway and regulate cell apoptosis. This is highly consistent with the conclusion of this study.

Effect of Acupotomy on Cervical Myocyte Apoptosis

Apoptosis refers to the autonomous and orderly death of cells controlled by genes, that is, programmed death. The main apoptotic pathways include membrane receptor pathway and mitochondrial apoptotic pathway. Both of these pathways can activate caspase family, degrade important intracellular proteins, and thereby exert regulatory effects on cells. Cells

undergoing apoptosis often have mitochondrial damage, and in severe cases, apoptotic body may appear. In the transmission electron microscopy observations of this study, mitochondrial damage was observed in the cervical myocytes after modeling, and a small number of apoptotic bodies were formed, which proved the objective existence of apoptosis in cervical myocytes after CS modeling. In PI3K/Akt signaling pathway, both Caspase9 and bcl2 are apoptosis-related factors. Bcl2 family can be divided into two major categories. One category is anti-apoptotic proteins, including bcl2 and bcl-xl, and the other category is pro-apoptotic proteins, including Bax, Bad. Bcl2 mainly exerts an inhibitory effect on apoptosis by altering the potential on the mitochondrial membrane and regulating the permeability of cell membrane.[43–45] Caspase9, as the initiator of apoptosis, triggers a cascade reaction after activation, activating apoptotic executors such as Caspase3, 6, and 7, and causing apoptosis.[46,47] The increased expression of Caspase9 and the decreased expression of bcl2 can aggravate cell apoptosis. In this study, after modeling, the mRNA and protein expressions of Caspase9 increased, while bcl2 decreased, indicating the apoptosis of cervical myocytes. This was reversed after acupotomy treatment, demonstrating the improvement effect of acupotomy on the apoptosis of CS cell myocytes.

Our study has several limitations. (1) In terms of multiple immunofluorescence and COIP, although the localization and qualitative detection of FGF7, FGF10 and KDR proteins in normal group and model group were carried out, it was proved that there was co-localization and binding among them. However, quantitative detection after protein binding was not carried out. In the future, the effects of modeling and treatment on their binding amounts should be further improved. (2) When demonstrating the effect of KDR in the treatment of CS, only knockdown was performed without overexpression. In the future, research on the overexpression of KDR can be carried out to enrich and improve the signal transduction mechanism of acupotomy.

In this study, by constructing rat CS model with dynamic and static imbalance and model of KDR knockdown, on the basis of demonstrating the therapeutic effect of acupotomy, KDR was knockdown to detect the signal transduction of downstream molecules, thereby illustrating the key role of KDR in the process of acupotomy treatment for CS. Ultimately, it was proved that acupotomy may mediate FGF7 and 10/KDR signaling axis, activates PI3K/Akt signaling pathway, and regulates apoptosis of cervical myocytes, thereby achieving the purpose of treating CS, as shown in Figure 6.

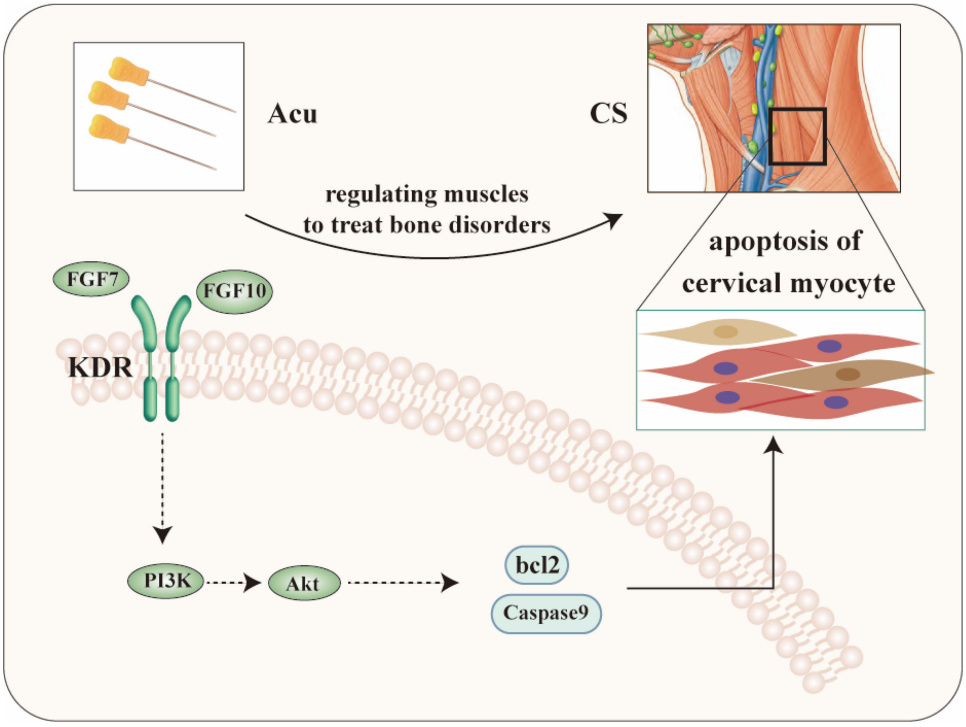

Figure 6 Mechanism of acupotomy for CS.

https://doi.org/10.2147/JPR.S557937

Data Sharing Statement

The data that support the findings of this study are available from the corresponding author upon reasonable request.

Author Contributions

All authors made a significant contribution to the work reported, whether that is in the conception, study design, execution, acquisition of data, analysis and interpretation, or in all these areas; took part in drafting, revising or critically reviewing the article; gave final approval of the version to be published; have agreed on the journal to which the article has been submitted; and agree to be accountable for all aspects of the work.

Funding

Supported by National Natural Science Foundation (No. 82360940), Natural Science Project of Jiangxi Province (No. 20224ACB206041 and No. 20232BAB216117) and the Advantageous Specialty Support Program of the Affiliated Hospital of Jiangxi University of Chinese Medicine (No. 0500750000225HX03).

Disclosure

All authors declare no conflicts of interest.

References

1. Wang C, Tian F, Zhou Y, et al. The incidence of cervical spondylosis decreases with aging in the elderly, and increases with aging in the young and adult population: a hospital-based clinical analysis. *Clin Interv Aging*. 2016;11(11):47–53. doi:10.2147/CIA.S93118
2. Fernández-de-Las-Peñas C, Alonso-Blanco C, Hernández-Barrera V, et al. Has the prevalence of neck pain and low back pain changed over the last 5 years? A population-based national study in Spain. *Spine J*. 2013;13(9):1069–1076.
3. Y SG, Choi J, J KH, et al. Global, Regional, and National Burden of Spine Pain, 1990-2019: a Systematic Analysis of the Global Burden of Disease Study 2019. *Arch Phys Med Rehabil*. 2024;105(3):461–469.
4. Shin DW, Shin JI, Koyanagi A, et al. Global, regional, and national neck pain burden in the general population, 1990-2019: an analysis of the global burden of disease study 2019. *Front Neurol*. 2022;955367.
5. Zhou FY, Liu FS, Fang T. Experiment research progress of acupotomy therapy for cervical spondylosis. *Chin. Arch. Tradit. Chin. Med*. 2019;37 (03):655–657.
6. Wong JJ, Shearer HM, Mior S, et al. Are manual therapies, passive physical modalities, or acupuncture effective for the management of patients with whiplash-associated disorders or neck pain and associated disorders? an update of the bone and joint decade task force on neck pain and its associated disorders by the OPTIMa collaboration. *Spine J*. 2016;16(12):1598–1630.
7. Abolfotouh SM, Alnori O, Choma T, et al. Epidemiology of Work-related neck pain among spine surgeons. *Global Spine J*. 2024;14(5):1515–1523.
8. Zhu QB, Gou P, Gou JJ. Clinical observation on the treatment of cervical spondylosis with needle knife. *Chin Acupuncture & Moxibustion*. 2010;30 (S1):12–13.
9. Zhang Y, Guo CQ. Acupotomy: the revival and innovation of acupuncture. *Chin Acupuncture & Moxibustion*. 2011;31(12):1111–1113.
10. Hu J, Tong H, Zhang J, et al. Acupotomy for musculoskeletal pain: exploring therapeutic potential and future directions. *J Pain Res*. 2025;18:3027–3036.
11. You JY, Liu FS, Chen MR. Discussion on the application of acupotomy in the prevention and treatment of cervical spondylosis based on muscles and bones theory. *CJTCMP*. 2022;37(02):753–755.
12. S LF, Fang T, Hong T, et al. Effects of acupotomy therapy on PI3K/Akt signaling pathway of posterior cervical extensor muscles cells in cervical spondylosis rabbits. *CJTCMP*. 2020;35(02):918–922.
13. J WY, Shi Q, W LW, et al. Cervical intervertebral disc degeneration induced by unbalanced dynamic and static forces: a novel in vivo rat model. *Spine*. 2006;31(14):1532–1538.
14. Yu JK, Wu YW, Dai XJ, et al. Experimental study on the biomechanical pathogenesis of cervical spondylosis. *J. Anhui Univ*. 1990;(01):47–51.
15. Livak KJ, Schmittgen TD. Analysis of relative gene expression data using real-time quantitative PCR and the 2(-Delta Delta C(T)) Method. *Methods*. 2001;25(4):402–408.
16. Folkman J, Shing Y. Angiogenesis. *J Biol Chem*. 1992;267(16):10931–10934.
17. Montesano R, D VJ, Baird A, et al. Basic fibroblast growth factor induces angiogenesis in vitro. *Proc Natl Acad Sci U S A*. 1986;83(19):7297–7301.
18. Peng M, F PM, Véronneau S, et al. Ontogeny of epidermal growth factor (EGF), EGF receptor (EGFR) and basic fibroblast growth factor (bFGF) mRNA levels in pancreas, liver, kidney, and skeletal muscle of pig. *Domest Anim Endocrinol*. 1997;14((5):286–294.
19. Stavri GT, Zachary IC, Baskerville PA, et al. Basic fibroblast growth factor upregulates the expression of vascular endothelial growth factor in vascular smooth muscle cells. Synergistic interaction with hypoxia. *Circulation*. 1995;92(1):11–14.
20. Hata Y, Rook SL, Aiello LP. Basic fibroblast growth factor induces expression of VEGF receptor KDR through a protein kinase C and p44/p42 mitogen-activated protein kinase-dependent pathway. *Diabetes*. 1999;48(5):1145–1155.
21. Lin YH, Chou LY, Chou HC, et al. The essential role of stathmin in myoblast C2C12 for vertical vibration-induced myotube formation. *Biomolecules*. 2021;11(11).
22. Liu X, Bai M, Sun Y, et al. FGF7-induced E11 facilitates cell-cell communication through connexin43. *Int J Biol Sci*. 2021;17(14):3862–3874.

23. Mitchell P, Steenstrup T, Hannon K. Expression of fibroblast growth factor family during postnatal skeletal muscle hypertrophy. *J Appl Physiol*. 1999;86(1):313–319.
24. Su W, Zheng X, Zhou H, et al. Fibroblast growth factor 10 delays the progression of osteoarthritis by attenuating synovial fibrosis via inhibition of IL-6/JAK2/STAT3 signaling in vivo and in vitro. *Mol Immunol*. 2023;159:46–57.
25. Liu FS, Qian JM, Fang T, et al. Effects of acupotomy on the expression of fibroblast growth factor family and its receptor in the splenius capitis muscles of rats with cervical spondylosis. *Chin J Tissue Eng Res*. 2025;29(18):3775–3783.
26. Ferrara N. Role of vascular endothelial growth factor in regulation of physiological angiogenesis. *Am J Physiol Cell Physiol*. 2001;280(6):C1358–C1366.
27. Peters KG, De Vries C, Williams LT. Vascular endothelial growth factor receptor expression during embryogenesis and tissue repair suggests a role in endothelial differentiation and blood vessel growth. *Proc Natl Acad Sci U S A*. 1993;90(19):8915–8919.
28. J CM, Dixelius J, Matsumoto T, et al. VEGF-receptor signal transduction. *Trends Biochem Sci*. 2003;28(9):488–494.
29. P GH, McMurtrey A, Kowalski J, et al. Vascular endothelial growth factor regulates endothelial cell survival through the phosphatidylinositol 3'-kinase/Akt signal transduction pathway. Requirement for Flk-1/KDR activation[J]. *J Biol Chem*. 1998;273(46):30336–30343.
30. Dudek H, Datta SR, Franke TF, et al. Regulation of neuronal survival by the serine-threonine protein kinase Akt. *Science*. 1997;275(5300):661–665.
31. Yao R, Cooper GM. Requirement for phosphatidylinositol-3 kinase in the prevention of apoptosis by nerve growth factor. *Science*. 1995;267(5206):2003–2006.
32. Minshall C, Arkins S, Freund GG, et al. Requirement for phosphatidylinositol 3'-kinase to protect hemopoietic progenitors against apoptosis depends upon the extracellular survival factor[J]. *J Immunol*. 1996;156(3):939–947.
33. Zhong Y, Yu PB. Angiogenesis redux: an overall protective role of VEGF/KDR signaling in the microvasculature in pulmonary arterial hypertension. *Arterioscler Thromb Vasc Biol*. 2023;43(10):1784–1787.
34. Han Y, Ren J, Bai Y, et al. Exosomes from hypoxia-treated human adipose-derived mesenchymal stem cells enhance angiogenesis through VEGF/VEGF-R. *Int J Biochem Cell Biol*. 2019;109:59–68.
35. Gurski F, Shirvanchi K, Rajendran V, et al. Anti-inflammatory and remyelinating effects of fexagratinib in experimental multiple sclerosis. *Br J Pharmacol*. 2025;182(1):142–161.
36. Liu X, Zhang Y, Sun X, et al. Di-(2-ethyl hexyl) phthalate induced oxidative stress promotes microplastics mediated apoptosis and necroptosis in mice skeletal muscle by inhibiting PI3K/AKT/mTOR pathway. *Toxicology*. 2022;474:153226.
37. Xu S, Li Y, Lu Y, et al. LZTS2 inhibits PI3K/AKT activation and radioresistance in nasopharyngeal carcinoma by interacting with p85. *Cancer Lett*. 2018;420:38–48.
38. Roy NK, Monisha J, Padmavathi G, et al. Isoform-specific role of akt in oral squamous cell carcinoma. *Biomolecules*. 2019;9(7):253.
39. Huang X, Liu G, Guo J, et al. The PI3K/AKT pathway in obesity and type 2 diabetes. *Int J Biol Sci*. 2018;14(11):1483–1496.
40. X LJ, F WS, W HY, et al. Research progress on treatment of alzheimers disease with traditional chinese medicine targeting PI3K/Akt signaling pathway. *Chin. Arch. Tradit. Chin. Med*. 2025;43(01):72–76.
41. LV X, Zhou DA. Research progress on the effects of the PI3K/AKT signaling pathway on skeletal muscle regeneration. *Chin J Sports Med*. 2020;39(11):908–912.
42. Li B, Wang Z, He Y, et al. Adropin improves radiation-induced myocardial injury via VEGFR2/PI3K/Akt pathway. *Oxid Med Cell Longev*. 2022;2022:8230214.
43. Arito M, Tsutiya A, Sato M, et al. Role of layilin in regulating mitochondria-mediated apoptosis: a study on B cell lymphoma (BCL)-2 family proteins. *BMC Mol Cell Biol*. 2024;25(1):24.
44. Kuzu B, Arzuk E. Discovery of new pyrazole-tosylamide derivatives as apoptosis inducers through BCL-2 inhibition and caspase-3 activation. *Chem Biodivers*. 2024;e202401673.
45. Zhang Q, Li X, He C, et al. Artesunate promotes cervical cancer cell apoptosis by regulating Bcl2 family molecules and reducing the mitochondrial membrane potential. *Oncol Lett*. 2024;28(1):315.
46. Fan TJ, Han LH, Cong RS, et al. Caspase family proteases and apoptosis. *Acta Biochim Biophys Sin*. 2005;37(11):719–727.
47. Batoon L, J KA, Kannan R, et al. Caspase-9 driven murine model of selective cell apoptosis and efferocytosis. *Cell Death Dis*. 2023;14(1):58